Evaluation of the frequency characteristics of cntTSP measurement for unsteady low-speed flow

OPEN ACCESS
IOP Publishing
Measurement Science and Technology
Meas. Sci. Technol. **34** (2023) 065301 (10pp)
https://doi.org/10.1088/1361-6501/acb8d0

Evaluation of the frequency characteristics of cntTSP measurement for unsteady low-speed flow

Tsubasa Ikami[1,2,*], **Yasufumi Konishi**[1] and **Hiroki Nagai**[1]

[1] Institute of Fluid Science, Tohoku University, Sendai, Japan
[2] Department of Aerospace Engineering, Tohoku University, Sendai, Japan

E-mail: tsubasa.ikami.s7@dc.tohoku.ac.jp

Received 14 December 2022, revised 23 January 2023
Accepted for publication 3 February 2023
Published 1 March 2023

Abstract

Carbon nanotube temperature-sensitive paint (cntTSP) is a fluid measurement technology that utilizes temperature-sensitive paint (TSP). It works as an optical temperature sensor, with a thin layer of carbon nanotubes to heat the TSP layer. This study investigated the frequency characteristics of cntTSP measurements in low-speed flow. The flow field on the flat plate was periodically changed by introducing intermittent local disturbances to the flat plate in a low-speed wind tunnel test. cntTSP measurement was conducted behind the local disturbance to evaluate changes in the temperature associated with periodic changes in the flow. The amplitude of the temperature change decreased approximately linearly with the frequency in a double-logarithmic graph. Moreover, the temperature amplitude at 25 Hz was 0.008 K, and it was necessary to detect a very small temperature change to evaluate high-frequency phenomena.

Keywords: carbon nanotubes temperature-sensitive paint, frequency characteristics, low-speed flow

(Some figures may appear in colour only in the online journal)

1. Introduction

Temperature-sensitive paint (TSP) is used to measure surface temperature fields. In this technique, the temperature is optically measured using temperature quenching of the luminophore in the paint [1]. TSP has received considerable attention as a flow measurement technique in wind tunnel tests, such as boundary layer transition [2–5] and aerodynamic heating measurements [6–8].

The heat transfer coefficient in a flow field depends on the flow state; for example, the turbulent flow has a higher heat transfer coefficient than the laminar flow owing to turbulent mixing. Therefore, when there is a temperature difference between the model surface and flow, the amount of heat exchange due to convection depends on the local heat transfer coefficient that reflects the flow state. The different local heat transfer coefficients cause a difference in the time change rate of the model surface temperature. In addition, the model surface temperature at thermal equilibrium differs between the flow states. In previous studies, infrared (IR) heaters [2, 5], hot water circulation systems [9], and the step temperature change in flow [3] were used to set the temperature difference between the model surface and the flow. A recent study has proposed carbon nanotube temperature-sensitive paint (cntTSP), in which a thin layer of carbon nanotube (CNT) is used to heat the TSP layer [10]. The CNT layer provides electrical resistance because CNTs have a high electrical conductivity. As a result, the CNT layer generates heat homogeneously on the model when a voltage is applied. This heat increases the temperature at the TSP layer, and the TSP measures the surface temperature. These characteristics of CNT heating allow

* Author to whom any correspondence should be addressed.

the simplification of the heating system and long-duration measurements.

cntTSP was proposed by Klein *et al* and was initially used to measure the boundary layer transitions in a transonic flow in a cryogenic wind tunnel test [10–12]. In a recent study, Bitter *et al* applied the cntTSP technique to measure the wake of a cylinder on a flat plate in transonic flow [13]. This study successfully captured the temperature change caused by Kármán vortex shedding at approximately 4300 Hz.

cntTSP measurement is also used in low-speed flows. Low-speed flows are often used to simulate low-Reynolds-number conditions. In addition, it is still technically challenging to employ pressure-sensitive paint to a low-speed flow because of its small pressure fluctuations. Yorita *et al* and Ikami *et al* quantitatively evaluated the static and quasi-static transition points on a wing model surface in low-speed wind tunnel tests using cntTSP [14–16]. Moreover, Ikami *et al* dynamically evaluated the motion of the transition points on a pitching airfoil under low-speed conditions [17]. This study measured the transition points on an airfoil moving at a maximum frequency of 4.2 Hz. However, this previous study also proposes to use the heat transfer coefficient to detect the transition points because the conventional method, which uses the temperature profile, cannot correctly evaluate the transition position owing to the very small temperature change. The temperature at the flow-interacted surface conducts in the thickness direction. This process causes a time delay and a decrease in the amplitude of the temperature change. Therefore, the temperature change is very small when the flow field changes periodically, as in the pitching airfoil. Thus, it is important to understand how the temperature change decreases with frequency to conduct unsteady cntTSP measurements.

Previous studies have investigated the response of TSP to measure the aerodynamic heating in hypersonic flows quantitatively. The measurement duration in a hypersonic wind tunnel is usually of the order of milliseconds. Therefore, the time response must be guaranteed to accurately evaluate the aerodynamic heating that occurs within such a short time. Nagai *et al* quantitatively evaluated aerodynamic heating on a cylinder and a flying object in a hypersonic wind tunnel test using TSP [18]. Nagayama *et al* measured the heat flux around a conical model in a shock tunnel using a TSP to visualize the boundary layer transition [19, 20]. In addition, Ozawa *et al* conducted TSP measurements in a high-enthalpy wind tunnel. They reported an unsteady phenomenon related to the boundary-layer transition on a conical model [21]. Horagiri and Nagai modeled instantaneous aerodynamic heating by external heating using a CO_2 laser and evaluated the quantitative time response of the TSP [22]. Their work calculated the heat flux using the time-series surface temperature. It evaluated the time response, assuming a first-order delay system. They investigated the influence of the thermal diffusivity and TSP layer thickness on the time response. They obtained a TSP with a time response of 0.205 ms under the fastest condition.

The model surface was exposed to a sudden external heat input in the aerodynamic heating measurement. Thus, previous studies have evaluated the temperature or heat flux response against the external step heat input. On the other hand, there is no external heat input owing to aerodynamic heating for low-speed flow, which is sufficiently slow compared to the speed of sound. However, the heat transfer coefficient at the surface changes for unsteady measurements at low speeds. In addition, the cntTSP measurement generates internal heat. Thus, the TSP layer is exposed to different boundary conditions for aerodynamic heating measurements in hypersonic flows and unsteady measurements in low-speed flows. It is necessary to establish a method to evaluate the response of the TSP in an unsteady measurement at low-speed flow rather than use the conventional method of time response evaluation assuming aerodynamic heating.

Simon *et al* evaluated the frequency characteristics of IR camera measurements at low-speed flows [23]. They introduced intermittent disturbances into the boundary layer using a loudspeaker on a flat plate, heated the flat plate in the downstream region, and measured the temperature change using an IR camera. In their study, the amplitude of the temperature change with an arbitrary frequency was obtained by changing the interval of intermittent disturbance. Consequently, they obtained the frequency-response curve of the IR camera measurements. The TSP and IR camera are temperature measurement systems, although they use different measurement principles. Therefore, a similar method is expected to be adapted to evaluate the frequency characteristics of cntTSP measurements in low-speed flow. This study establishes the methodology to evaluate the frequency characteristic of cntTSP measurements for periodic flow-field changes in a low-speed flow and reveals it.

2. Methodology

2.1. Carbon nanotubes temperature-sensitive paint

TSP is a temperature measurement technique used in wind tunnel experiments. TSP is a paint mixture of a luminophore that functions as a temperature sensor, a polymer that adheres the luminophore to the model surface, and a solvent that dissolves the luminophore and polymer. The luminophore of TSP is excited by light at specific wavelengths, such as blue and ultraviolet wavelengths, and emits luminescence. The luminescence intensity decreases at high temperatures because of temperature quenching. Therefore, the temperature can be measured optically by acquiring luminescence intensity using a photodetector.

cntTSP is an applied TSP technique that uses a thin CNT layer to heat the TSP layer. CNT are carbon allotropes with a nanoscale cylindrical structure and high electrical conductivity [24]. A thin CNT layer was formed on the model by spraying a mixture of CNT powder, polymer binder, and solvent.

Figure 1 shows the flow field measurement principle of the cntTSP. Three layers (CNT, screen, and TSP) were coated onto the model. The CNT layer was connected to the power supply, and a voltage was applied, resulting in Joule heat. This heat reaches the TSP layer through the screen layer, causing heat exchange between the TSP surface and the flow. Therefore, a temperature distribution that reflects the flow state is formed on the model. Corresponding to the temperature

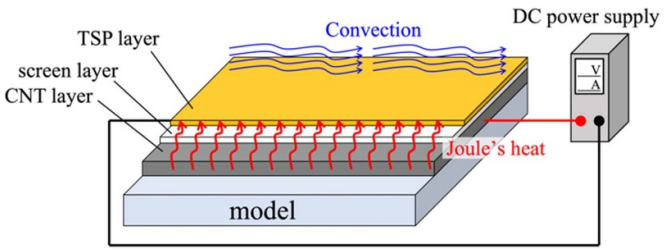

Figure 1. Principle of cntTSP measurement.

distribution, the TSP changes the luminescence intensity, which can be detected by a high-speed camera to obtain high-spatial-resolution data at high sampling rates.

2.2. *Wind tunnel experiment*

This study establishes a method for evaluating the frequency characteristics of cntTSP measurements in a low-speed wind tunnel test. The methodology of the wind tunnel test and data processing are described in this section.

2.2.1. Wind tunnel and test section. The experiment was performed in a small low-turbulence wind tunnel at the Institute of Fluid Science, Tohoku University. The wind tunnel was of the Göttingen type. An open-type test section was used in this study. The test section length was 897 mm, and the nozzle outlet had a regular octagon cross-section with a width of 293 mm.

Figure 2 shows a schematic of the test section setup and the size of the flat plate. A flat plate was placed horizontally in the flow at the test section. The flat plate had a length, width, and thickness of 600, 355, and 15 mm, respectively. The flat plate was made of aluminum. The area 100 mm from the leading edge had an elliptical cross-section with an aspect ratio of 20:3. A 1 mm diameter hole was placed 200 mm from the leading edge as an outlet for the disturbance. In addition, a cntTSP layer with a length of 140 mm and width of 100 mm was coated 5 mm downstream from the hole. The cntTSP-coated area and the surrounding area were made of acrylic for electric isolation. A loudspeaker (FF165WK, Fostex) is placed outside the test section under a flat plate. The loudspeaker was then covered with an acrylic plate. A hole was also installed on the acrylic cover and connected to a hole on a flat plate via a silicon tube. Thus, the disturbances generated by the loudspeaker propagate up to the hole on the flat plate. The disturbance signals were created as a white noise using a multifunction I/O device (USB-6363, National Instruments) and amplified using a power amplifier (Power Amplifier XP 1000, YAMAHA) before being input to the loudspeaker.

A hot-wire anemometer was placed 145 mm behind the disturbance outlet and 1.5 mm above the flat plate. A single-sensor probe (miniature wire probe, boundary layer (55P15), Dantec Dynamics) was used as the hot-wire probe. The sensitive part of this probe was made of tungsten, with a diameter of 5 μm and a length of 1.25 mm. The probe was connected to a constant-temperature hot-wire anemometer (CTA-002,

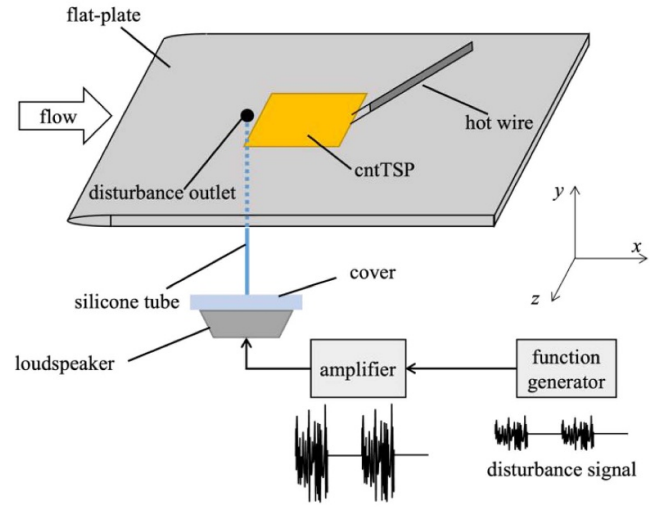

(a) Setup of the test section.

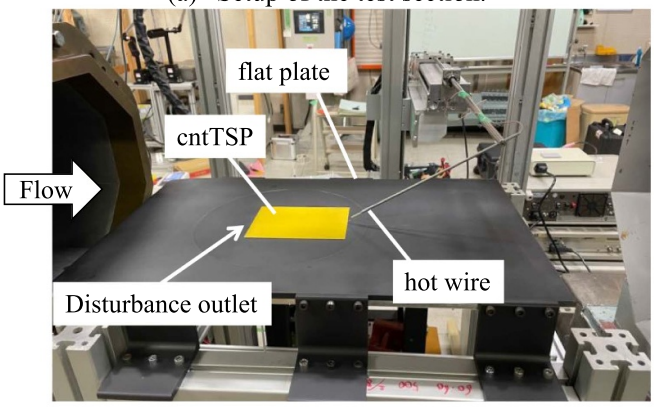

(b) Picture of the test section and cntTSP coating.

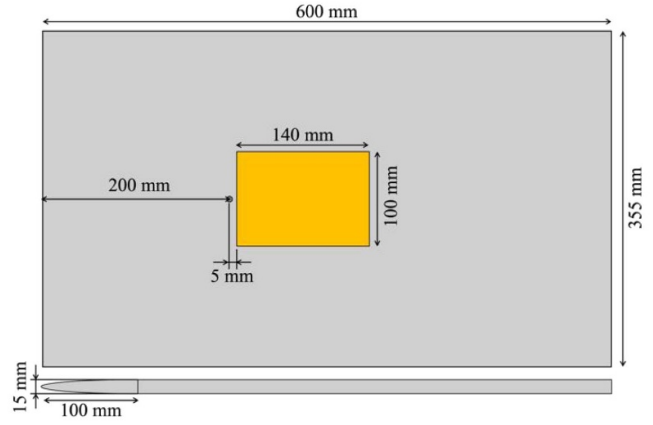

(c) Size of the flat plate.

Figure 2. Sketch and picture of the test section.

Institute of Flow Research) to maintain a constant temperature in the sensitive part.

2.2.2. cntTSP coating and optical setup. The cntTSP formulation is listed in table 1. Polymethylmethacrylate was used as a polymer binder for the CNT, screen, and TSP layers. For the CNT layer, a commercially available CNT (HD-CNT, Microphase) was used. The screen layer was mixed

Table 1. Formulation of the cntTSP layers.

CNT layer		
Solvent	Dichloromethane	100 ml
Polymer	Polymethylmethacrylate	500 mg
Conductor	CNTs	500 mg
Screen layer		
Solvent	Dichloromethane	100 ml
Polymer	Polymethylmethacrylate	1000 mg
White coloring	Boron nitride	1400 mg
TSP layer		
Solvent	Dichloromethane, Ethanol	20 ml, 10 ml
Polymer	Polymethylmethacrylate	400 mg
Luminophore	Ru-phen	40 mg

with boron nitride to obtain a white color. Dichlorotris (1,10-phenanthroline) ruthenium(II) hydrate (Ru-phen) was used as the luminophore for the TSP layer [25]. Copper tape with a width of 5 mm was used for the electrical connections to the CNT layer. The approximate thickness of each layer was 30 μm for the CNT layer, 25 μm for the screen layer, and 5 μm for the TSP layer.

Figure 3 shows the optical setup for cntTSP measurements. A high-speed video camera (FASTCAM SA-X2, Photron) was used as the photodetector for the TSP luminescence. A single focal-length lens (Nikkor 50 mm f/1.4, Nikon) and an optical bandpass filter (575 nm CWL, 50 mm Dia. Hard Coated OD 4.0 50 nm Bandpass Filter, Edmund Optics) were attached to the camera. The peak wavelength of the luminescence of Ru-phen was 580 nm [1], and the optical bandpass filter had a central wavelength of 575 nm and a full-width-at-half-maximum of 50 nm. The f-number of the lens was set to 1.4. The resultant spatial resolution was 4 pixels mm^{-1}. Two blue light-emitting diodes (LEDs) (IL-106B LED, HARDsoft Microprocessor Systems) were used as the excitation light sources for the TSP. The center wavelength of the light source was 462 nm, corresponding to the excitation wavelength peak of Ru-phen at approximately 450 nm [1]. Athermanous filters (HAF-50 S-30 H, Sigma Koki) and bandpass filters (SV0510, Asahi Spectra) were attached to blue LEDs to avoid the radiant heat from the LEDs.

2.2.3. Test conditions. The test conditions are listed in table 2. Local disturbances were intermittently introduced into the boundary layer. The intermittent disturbances were introduced with a duty ratio of 0.5. The interval between the introduction of disturbances and the estimated frequency of the fluctuations in the flow field can be expressed by equation (1).

$$f_{\mathrm{est}}[\mathrm{Hz}] = \frac{1}{\text{interval of disturbance}[\mathrm{s}]}. \tag{1}$$

Here, the lifetime of Ru-phen, the TSP, is 1.4 μs [1], which is sufficiently short compared to the estimated flow-field fluctuations.

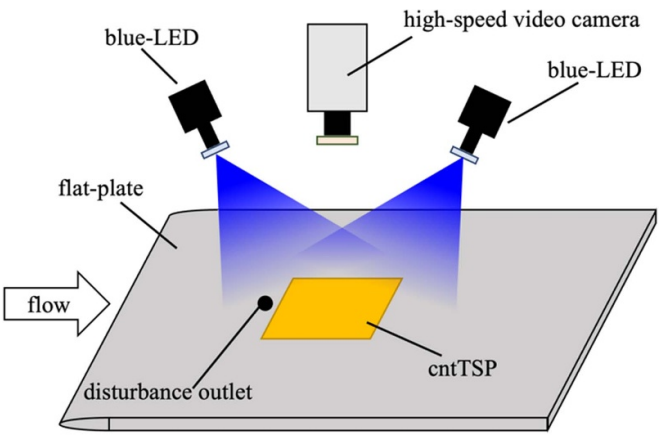

Figure 3. Sketch of the optical setup.

Table 2. Test conditions of cntTSP measurement.

Interval of disturbance (estimated frequency)	4, 2, 1.33, 1, 0.4, 0.2, 0.133, 0.1, 0.04 s (0.25, 0.5, 0.75, 1, 2.5, 5, 7.5, 10, 25 Hz)
Frame rate	5000 fps
Exposure time	1/5071 s
The number of images	84 403
Measurement duration	Approx. 16.9 s

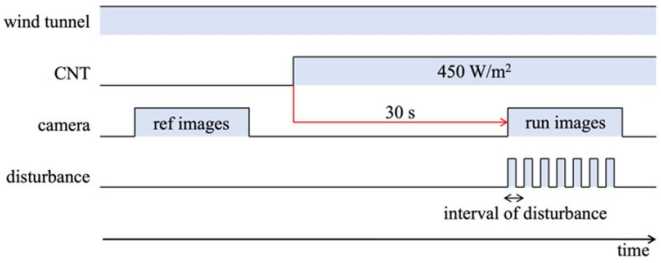

Figure 4. Data acquisition procedure.

The flow velocity was set at 10 m s^{-1}. The Reynolds number based on the distance from the leading edge was 1.3 × 10^5–2.2 × 10^5 in the cntTSP area, which is below the critical Reynolds number.

The image acquisition procedure is illustrated in figure 4. The TSP measurements were performed using the intensity method. The intensity method requires two types of images: reference and run images. The reference image acquisition was performed at room temperature without CNT heating, and cntTSP was sufficiently exposed to the wind tunnel flow. Disturbances were not introduced in the reference image acquisition. After the reference image acquisition, a voltage was applied to the CNT layer to start CNT heating. The direct-current power applied a voltage to the CNT layer, resulting in a heat input of 450 W m^{-2}. The run image acquisition started 30 s after the start of heating. These conditions were determined after preliminary tests confirmed that a sufficient temperature rise occurs on the plate to be measured by the TSP.

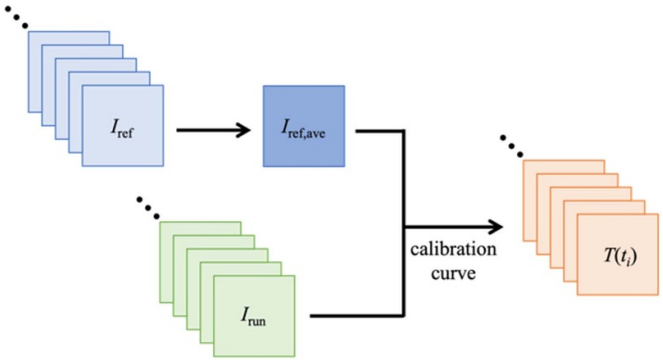

Figure 5. Image processing procedure.

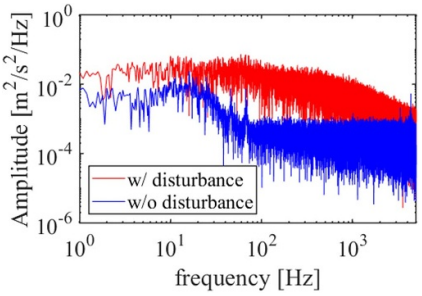

Figure 6. Comparison of frequency spectrums between the conditions w/ and w/o the disturbance.

The run image acquisition and disturbance introduction started simultaneously.

In addition to the cntTSP measurement, the hot-wire anemometer measurement was also performed simultaneously. A low-pass filter was applied to the hot-wire anemometer signal with a cut-off frequency 40 kHz to filter out high-frequency components. The filtered signals were obtained with a sampling frequency of 10 kHz and 18 s via an analog-to-digital converter on a multifunction I/O device (USB-6363, National Instruments).

2.2.4. Data processing. Figure 5 shows the image-processing procedure. In the intensity method, the temperature can be calculated from the ratio of the reference image I_{ref} to the run image I_{run}, using the calibration result. First, all acquired reference images were averaged to improve the signal-to-noise ratio. The instantaneous temperature $T(t_i)$ was then calculated using the instantaneous run image $I(t_i)$ and the averaged reference image $I_{ref,ave}$. The calibration curve was obtained from a prior calibration test.

3. Results and discussion

3.1. Periodic change in flow field

First, the changes in the flow field due to the introduction of disturbances are discussed. Figure 6 shows the frequency spectra of the velocity fluctuation obtained by the hot-wire anemometer for conditions with and without disturbances. The hot-wire anemometer was placed in the boundary layer, where 145 mm behind the disturbance outlet and 1.5 mm above the flat plate. Here, the disturbance was introduced continuously for the condition with disturbance. The amplitudes in the condition without disturbance were lower than those in the disturbance condition over a wide range. In particular, the amplitudes were lower than the circuit noise in the high-frequency region above 100 Hz without disturbance. On the other hand, with continuous disturbance, the amplified broadband spectrum. This characteristic in the frequency spectra shows that the introduction of the disturbance leads to an increase in broadband turbulence in the boundary layer on the flat plate.

Next, changes in the flow field caused by intermittent disturbances are discussed. Figure 7 shows the velocity fluctuations and frequency spectra acquired using the hot-wire anemometer. u' is the time-dependent flow fluctuation. t^* is the time normalized by the interval of intermittent disturbances. Figure 7 shows (a) $f_{est} = 0.25$ Hz, (b) $f_{est} = 2.5$ Hz, and (c) $f_{est} = 25$ Hz cases on behalf of the test conditions. The dashed lines in the frequency spectra of figure 7 indicate f_{est}. The velocity fluctuations showed repetitions of large and small fluctuations corresponding to the disturbance interval. The duty ratio of the large and small fluctuation parts may be longer than 0.5, especially in high-frequency conditions, while the duty ratio of the intermittent disturbances was 0.5. However, the influence of the shift of the duty ratio was small enough to be negligible in the following discussion on temperature changes. The frequency spectra also show the sharp peaks at f_{est} for all conditions. The dominant peaks are obtained at f_{est}, indicating that the intermittent disturbance introduces arbitrary frequency fluctuations to the flow field.

Moreover, the turbulent intensity is calculated for each intermittent disturbance condition. The turbulent intensities are within $7.3 \pm 0.4\%$ for all conditions, and no significant difference is observed in the turbulent intensity. The temperature fluctuations caused by intermittent disturbances are influenced only by their intervals (i.e. f_{est}) because the heating conditions are the same for the cntTSP measurements, the main flow velocities are the same for all test conditions, and the turbulent intensities are similar.

3.2. Temperature distribution

Figure 8 shows the time-averaged temperature distribution. The flow direction is from left to right. Only the area heated by the CNT layer is shown in figure 8. ΔT is the temperature increase due to CNT heating. Figure 8(a) shows the temperature distribution when CNT heating is applied without flow and disturbance. ΔT is slightly lower on the upstream and downstream sides of the measured area. These areas are in contact with the unheated areas of the flat plate, resulting in a heat leak.

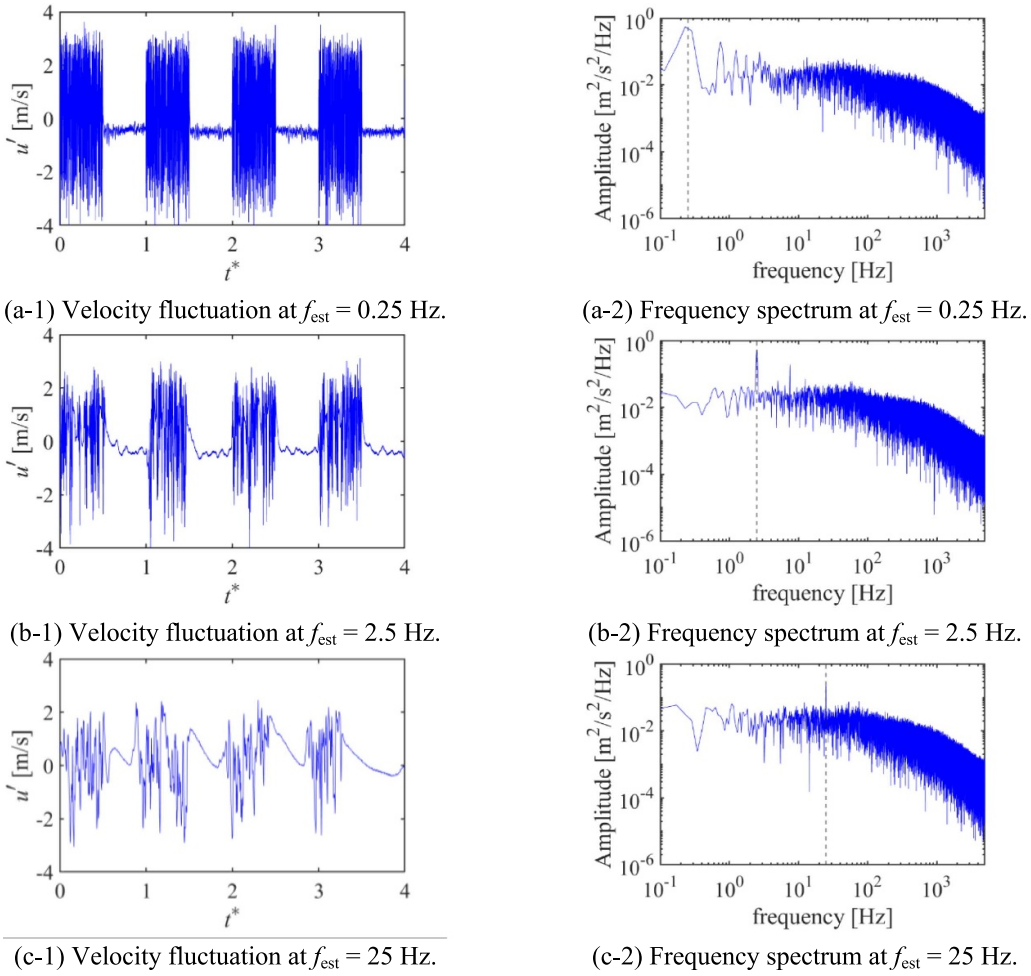

(a-1) Velocity fluctuation at f_{est} = 0.25 Hz. (a-2) Frequency spectrum at f_{est} = 0.25 Hz.

(b-1) Velocity fluctuation at f_{est} = 2.5 Hz. (b-2) Frequency spectrum at f_{est} = 2.5 Hz.

(c-1) Velocity fluctuation at f_{est} = 25 Hz. (c-2) Frequency spectrum at f_{est} = 25 Hz.

Figure 7. Flow field change due to the introduction of intermittent disturbance.

Figures 8(b)–(d) show the time-averaged temperature distribution with flow and intermittent disturbances. Figure 8(e) is the temperature distribution in the without-disturbance case. The overall ΔT decreases compared with the heating-only condition, as shown in figure 8(a). The temperature is lower in the upstream region and increases gradually in the downstream region. This is because the thermal boundary layer has not yet developed in the upstream region, resulting in a large heat exchange and small ΔT. A similar temperature distribution is also observed in the without-disturbance case in figure 8(e). In addition, a lower ΔT is observed behind the disturbance outlet compared with the other areas in figures 8(b)–(d). In this area, the introduction of the disturbance causes a larger heat exchange with the flow owing to turbulent mixing.

3.3. Singular value decomposition and mode selection

The temperature change caused by the intermittent local disturbances was too small compared to the ΔT caused by CNT heating. Then, singular value decomposition (SVD) [26] was applied to the time-series temperature field to reduce noise and extract small temperature changes. In SVD, dataset $\mathbf{X}$ is decomposed into the left-singular vectors $\mathbf{U}$ representing spatial correlations, the singular values $\mathbf{\Sigma}$ representing the contribution of each mode, and the right-singular vectors $\mathbf{V}$ representing the temporal variation of each mode, as shown in equation (2).

$$\mathbf{X} = \mathbf{U}\Sigma\mathbf{V}^{*}. \tag{2}$$

Here, $\mathbf{V}^{*}$ is the adjoint matrix of $\mathbf{V}$. Each left- and right-singular vector is a unit vector. Dataset $\mathbf{X}$ was created by rearranging the temperature distribution into a vector form, where the rows represent the temporal evolution, and the columns represent the spatial distribution.

Using the evaluation method of the singular value thresholding by Gavish and Donoho [27], the 20th mode was selected as the threshold in the largest case for the data obtained in this experiment. Therefore, the first 32 modes were maintained to select the mode from a large enough number of modes, and the lower modes were truncated to reduce noise.

Next, the modes representing the change in the temperature field caused by intermittent disturbances were selected from the first 32 modes, which were maintained by the threshold. Regarding the mode selection, Pastuhoff *et al* [28] selected modes in terms of the spatial distribution and

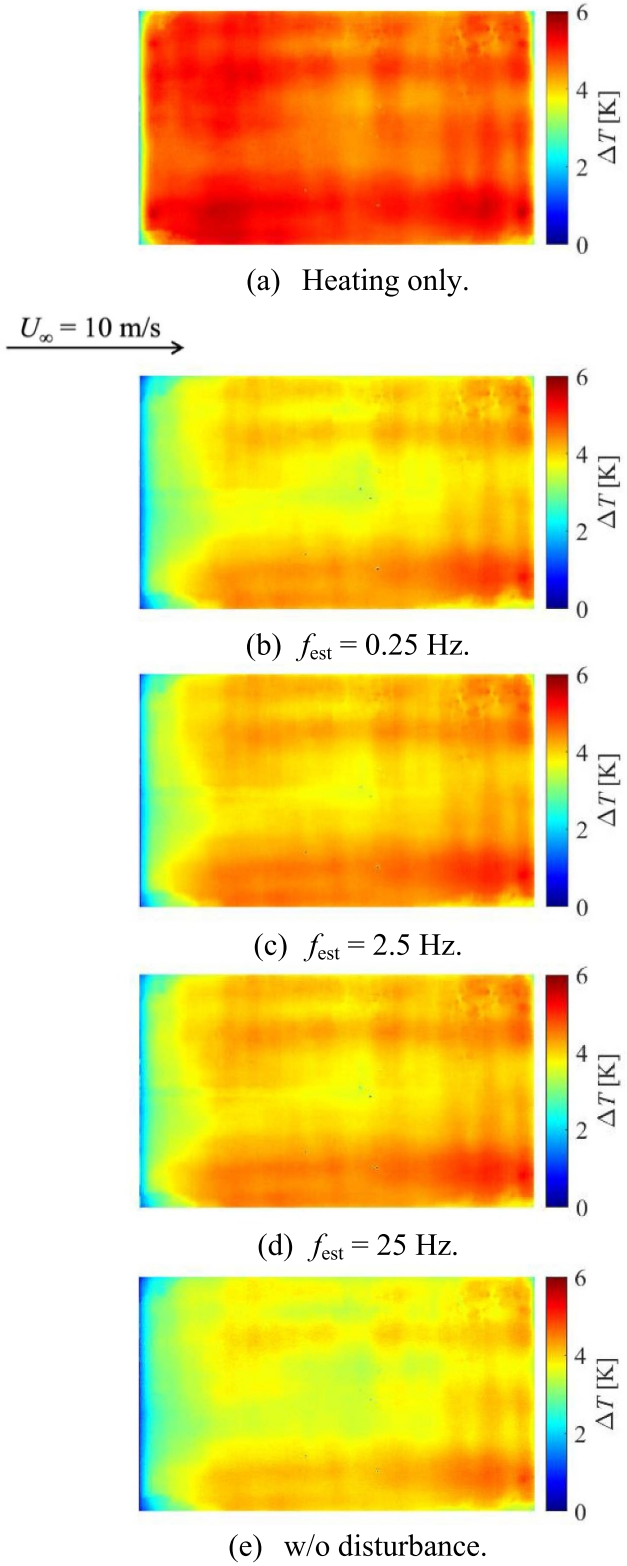

Figure 8. Temperature distribution.

temporal variation of phenomena occurring in the flow field. In addition, Sugioka *et al* [29] proposed a method to select a mode in which the frequency spectrum of the mode coincides with the flow field measured using another method. Inoue *et al* [30] proposed a method for determining the amplitude of the mode using sparse modeling and automatically selecting the mode.

In this study, it is expected that temperature changes occur only in a wedge-shaped region because the turbulent wedge is formed behind the disturbance outlet. Moreover, the temperature change coincides with the interval of intermittent disturbances. Therefore, following Pastuhoff *et al* [28], the modes were selected to satisfy the following criteria.

(a) The mode exhibits a wedge-shaped spatial characteristic.
(b) The frequency spectrum of the time variation of the mode exhibits a predominant peak at the estimated frequency of the intermittent disturbance.

Figure 9 shows the selected modes and frequency spectra of the amplitudes. Figure 9 shows the representative selected mode for (a) f_{est} = 0.25 Hz, (b) f_{est} = 2.5 Hz, and (c) f_{est} = 25 Hz. The left-singular vector is rearranged from the vector form to the original arrangement. The dashed lines in figure 9 represent f_{est}.

First, the spatial structure shows a turbulent wedge in the left-singular vectors for all conditions. These results show that the location of the turbulent wedge and its spatial features are the same, although the intervals of the intermittent disturbances are different. Thus, the flow conditions are the same except for the temporal or frequency feature for all intermittent disturbance conditions.

In the frequency spectra, distinct peaks appear at f_{est}. This is consistent with observations made using the hot-wire anemometer. In addition, the low amplitudes at high frequencies above approximately 100 Hz are noise from the camera sensor and the background. These spatiotemporal characteristics indicate that the temperature field changes with the frequency of the f_{est} and the spatial distribution corresponding to the turbulent wedge.

3.4. Amplitude of temperature change and frequency characteristics

In this section, the temperature changes associated with intermittent disturbances are evaluated quantitatively. Time-series temperature fields were reconstructed using the selected mode. The root mean square (RMS) of the reconstructed time-series temperature was calculated and defined as the amplitude of temperature change. Figure 10 shows the distribution of the RMS values. Note that the ranges of the color bars are different for each frequency condition. The large RMS values are limited to the wedge-shaped region, indicating that the temperature changed only in this region.

Here, the average value in the black square area shown in figure 10 is used as the representative RMS value for each condition. The local Reynolds number was 2.2×10^5 in this region. Moreover, according to the temperature distributions in figure 8, there is no need to consider the low-temperature region on the upstream side and the heat leakage to the flat

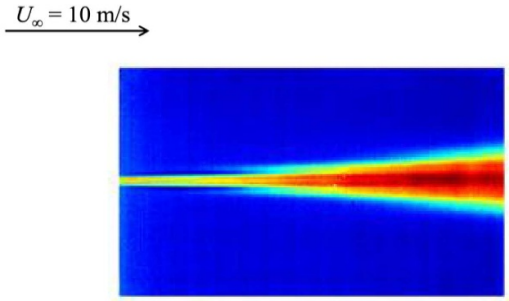

(a-1) Selected left-singular vector for f_{est} = 0.25 Hz

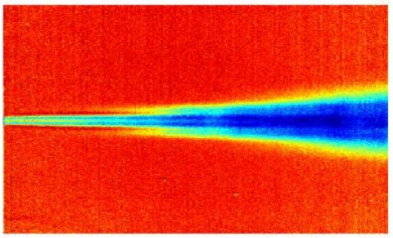

(b-1) Selected left-singular vector for f_{est} = 2.5 Hz

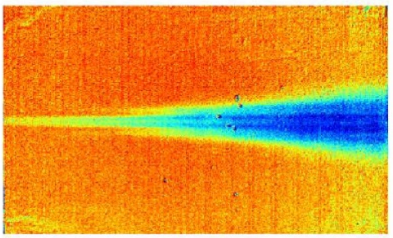

(c-1) Selected left-singular vector for f_{est} = 25 Hz

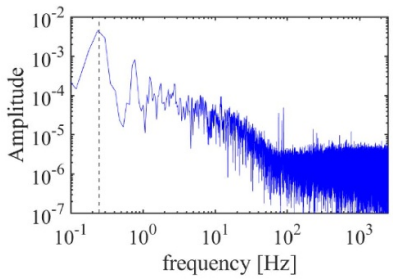

(a-2) Frequency spectrum of the selected right-singular vector for f_{est} = 0.25 Hz

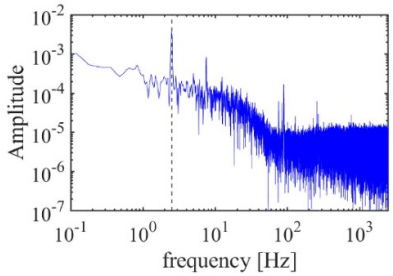

(b-2) Frequency spectrum of the selected right-singular vector for f_{est} = 2.5 Hz

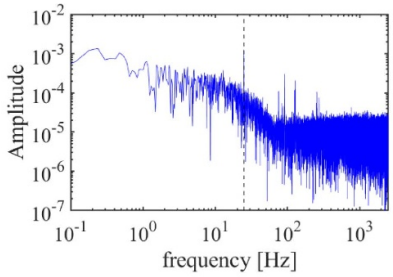

(c-2) Frequency spectrum of the selected right-singular vector for f_{est} = 25 Hz

Figure 9. Spatial and frequency characteristics of selected modes.

plate. It is also located downstream of the disturbance outlet and is expected to exhibit well-developed turbulence. The standard deviations of the values in black squares are treated as error bars. In addition, the area enclosed by the red square outside the turbulence wedge in figure 10 is selected to show the noise floor. The size of each square is 21 × 21 pixels, and 441 pixels are included here. Figure 11 shows the values of the temperature changes at the representative position (black box) and noise floor (red box). Figure 11 shows a double logarithmic graph. The same measurements at f_{est} = 1 Hz were performed twice to check the repeatability of the measurement. Thus, figure 11 includes two data points at f_{est} = 1 Hz, and the difference between the data was in the error bar. This result supports the repeatability of this experiment. Moreover, the noise floor is approximately 0.004 K for all the frequency conditions. In contrast, the temperature amplitude is 0.012 K at 25 Hz, and the noise floor corresponds to 32%. Therefore, the temperature amplitude was corrected by subtracting the noise floor value from the representative value.

Figure 12 shows the corrected temperature amplitudes. As shown in figure 12, the temperature amplitude decreases linearly with an increase in frequency on the double-logarithmic graph. The amplitude was 0.051 K at 0.25 Hz, 0.015 K at 2.5 Hz, and 0.008 K at 25 Hz, respectively. The slope of this decrease is that the amplitude decreases by 0.36 times for every ten-fold increase in frequency. It is considered that flow-field changes in the higher frequency cause temperature change only in a very thin layer on the surface, and this leads to a decrease in temperature changes.

The frequency characteristics of cntTSP measurement can be evaluated as the slope of the decrease in the temperature amplitude, as shown in figure 12. This slope can be used to evaluate the frequency characteristic of the cntTSP measurement. The frequency characteristic is evaluated as high when the slope is slow because the degradation in amplitude is suppressed even at high frequencies. On the other hand, the frequency characteristic is inferior when the slope is steep. Furthermore, for accurate measurement, it is necessary to

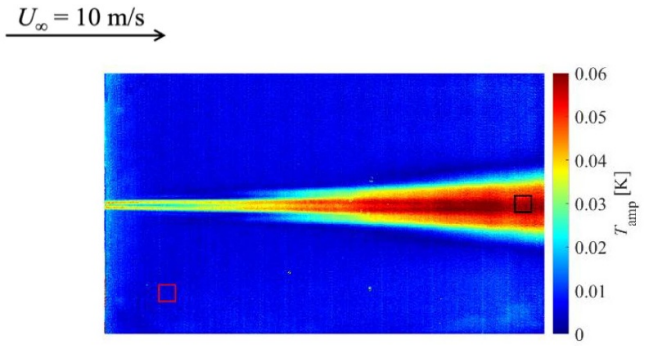

(a) $f_{est} = 0.25$ Hz

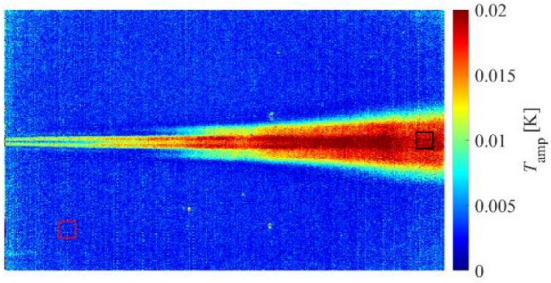

(b) $f_{est} = 2.5$ Hz

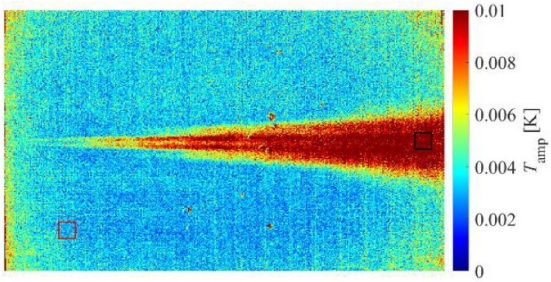

(c) $f_{est} = 25$ Hz

Figure 10. Amplitude of temperature change.

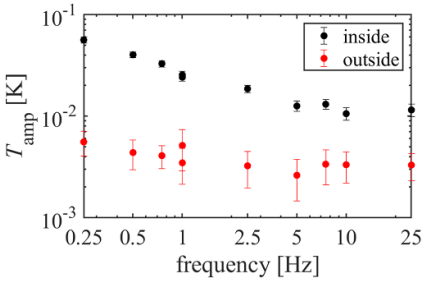

Figure 11. Raw amplitude and noise floor.

focus not only on the frequency characteristic but also on the magnitude of the temperature change itself. The present study revealed that wedge-shaped temperature changes were captured, even at 25 Hz, while the signal-to-noise ratio was low. However, the measurement conditions must be set so

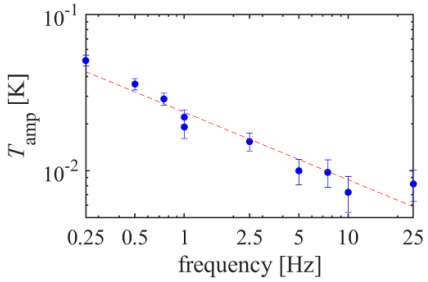

Figure 12. Frequency characteristics of the corrected amplitude of temperature change.

that the temperature amplitude becomes large, and the signal-to-noise ratio must be improved to capture higher-frequency phenomena.

4. Conclusion

In this study, an evaluation method to investigate the frequency characteristics of cntTSP measurements adequate to low-speed wind tunnel test was developed. Local disturbances were intermittently introduced into the boundary layer to change the flow field intermittently. The frequency characteristics were evaluated by measuring the temperature changes caused by the changes in the flow field. This study revealed that the temperature amplitude decreased approximately linearly with the frequency in a double-logarithmic graph. This characteristic is necessary for unsteady cntTSP measurements that measure periodic changes in the flow field. Moreover, the temperature change could be captured even at 25 Hz, which was the highest frequency condition in this study. However, it is necessary to accurately measure extremely small temperature changes for high-frequency phenomena. Future studies need to consider the thermal properties of cntTSP, such as the layer thickness and the polymer material, and the measurement conditions, such as the heat input of the CNT layer and the model material, to improve its frequency characteristics and increase its temperature changes.

Data availability statement

The data that support the findings of this study are available upon request from the authors.

Acknowledgments

This work was supported by JSPS KAKENHI (Grant Nos. JP22J12531 and JP21H01524). The authors would like to thank Mr T Takahashi and Mr H Okuizumi for their support during the wind tunnel tests.

ORCID iDs

Tsubasa Ikami https://orcid.org/0000-0002-6423-3394
Yasufumi Konishi https://orcid.org/0000-0002-8079-0051

References

[1] Liu T, Sullivan J P, Asai K, Klein C and Egami Y 2021 *Pressure and Temperature Sensitive Paints* (Cham: Springer)

[2] Ikami T, Fujita K and Nagai H 2021 Low-Reynolds-number flowfield of wing with control surface in propeller slipstream *J. Aircr.* **58** 228–35

[3] Fey U, Engler R, Egami Y, Iijima Y, Asai K, Jansen U and Quest J 2003 *20th Int. Congress on Instrumentation in Aerospace Simulation Facilities* (*Gottingen, Germany*)

[4] Costantini M, Henne U, Risius S and Klein C 2021 A robust method for reliable transition detection in temperature-sensitive paint data *Aerosp. Sci. Technol.* **113** 106702

[5] Yorita D, Asai K, Klein C, Henne U and Schaber S 2012 *50th AIAA Aerospace Sciences Meeting including the New Horizons Forum and Aerospace Exposition* (Nashville, TN: AIAA) (https://doi.org/10.2514/6.2012-1187)

[6] Ishiguro Y, Nagai H, Asai K and Nakakita K 2007 *45th AIAA Aerospace Sciences Meeting and Exhibit* (*Reno, NV, USA*) (https://doi.org/10.2514/6.2007-118)

[7] Ha S, Nagai H and Asai K 2010 *The 14th Int. Symp. on Flow Visualization, (ISFV14)* (*Daegu, Korea*)

[8] Nagai H, Horagiri T, Tanno H and Komuro T 2014 *The 16th Int. Symp. on Flow Visualization, (ISFV16)* (*Okinawa, Japan*)

[9] Capone A, Klein C, Di Felice F, Beifuss U and Miozzi M 2015 Fast-response underwater TSP investigation of subcritical instabilities of a cylinder in crossflow *Exp. Fluids* **56** 196

[10] Klein C, Henne U, Sachs W, Beifuss U, Ondrus V, Bruse M, Lesjak R and Löhr M 2014 *AIAA SciTech Forum* (National Harbor, MD: AIAA) (https://doi.org/10.2514/6.2014-1482)

[11] Klein C, Henne U, Sachs W, Beifuss U, Ondrus V, Bruse M, Lesjak R, Löhr M, Becher A and Zhai J 2015 *AIAA SciTech Forum* (Kissimmee, FL: AIAA) (https://doi.org/10.2514/6.2015-1558)

[12] Klein C, Henne U, Yorita D, Ondrus V, Beifuss U, Hensch A-K and Quest J 2017 *AIAA SciTech Forum* (Grapevine, TX: AIAA) (https://doi.org/10.2514/6.2017-0336)

[13] Bitter M, Hilfer M, Schubert T, Klein C and Niehuis R 2022 An ultra-fast TSP on a CNT heating layer for unsteady temperature and heat flux measurements in subsonic flows *Sensors* **22** 657

[14] Yorita D, Lemarechal J, Klein C, Fujita K and Nagai H 2018 *The 18th Int. Symp. on Flow Visualization* (*Zurich, Switzerland*) (https://doi.org/10.3929/ethz-b-000279205)

[15] Yorita D, Lemarechal J, Klein C, Fujita K and Nagai H 2020 *AIAA Scitech 2020 Forum* (Orlando, FL: AIAA) (https://doi.org/10.2514/6.2020-0296)

[16] Ikami T, Fujita K, Nagai H and Yorita D 2021 *AIAA Scitech 2021 Forum (Virtual Event)* (AIAA) (https://doi.org/10.2514/6.2021-0329)

[17] Ikami T, Fujita K, Nagai H and Yorita D 2021 Measurement of boundary layer transition on oscillating airfoil using cntTSP in low-speed wind tunnel *Meas. Sci. Technol.* **32** 075301

[18] Nagai H, Ohmi S, Asai K and Nakakita K 2008 Effect of temperature-sensitive-paint thickness on global heat transfer measurement in hypersonic flow *J. Thermophys. Heat Transfer* **22** 373–81

[19] Nagayama T, Nagai H, Tanno H and Komuro T 2016 *54th AIAA Aerospace Sciences Meeting* (San Diego, CA: AIAA) (https://doi.org/10.2514/6.2016-0358)

[20] Nagayama T, Nagai H, Tanno H and Komuro T 2017 *55th AIAA Aerospace Sciences Meeting* (Grapevine, TX: AIAA) (https://doi.org/10.2514/6.2017-1682)

[21] Ozawa H, Laurence S J, Schramm J M, Wagner A and Hannemann K 2015 Fast-response temperature-sensitive-paint measurements on a hypersonic transition cone *Exp. Fluids* **56** 1853

[22] Horagiri T and Nagai H 2014 *52nd Aerospace Sciences Meeting* (National Harbor, MD: AIAA) (https://doi.org/10.2514/6.2014-1408)

[23] Simon B, Filius A, Tropea C and Grundmann S 2016 IR thermography for dynamic detection of laminar-turbulent transition *Exp. Fluids* **57** 93

[24] Iijima S 1991 Helical microtubules of graphitic carbon *Nature* **354** 6348

[25] Ikami T, Fujita K and Nagai H 2022 Influence of formulations on characteristics of ruthenium-based temperature-sensitive paints *Sensors* **22** 901

[26] Taira K, Brunton S L, Dawson S T M, Rowley C W, Colonius T, McKeon B J, Schmidt O T, Gordeyev S, Theofilis V and Ukeiley L S 2017 Modal analysis of fluid flows: an overview *J. Am. Inst. Aeronaut. Astronaut.* **55** 12

[27] Gavish M and Donoho D L 2014 The optimal hard threshold for singular values is $4/\sqrt{3}$ *IEEE Trans. Inf. Theory* **60** 8

[28] Pastuhoff M, Yorita D, Asai K and Alfredsson P H 2013 Enhancing the signal-to-noise ratio of pressure sensitive paint data by singular value decomposition *Meas. Sci. Technol.* **24** 075301

[29] Sugioka Y, Hiura K, Chen L, Matsui A, Morita K, Nonomura T and Asai K 2019 Unsteady pressure-sensitive-paint (PSP) measurement in low-speed flow: characteristic mode decomposition and noise floor analysis *Exp. Fluids* **60** 108

[30] Inoue T, Matsuda Y, Ikami T, Nonomura T, Egami Y and Nagai H 2021 Data-driven approach for noise reduction in pressure-sensitive paint data based on modal expansion and time-series data at optimally placed points *Phys. Fluids* **33** 077105